# Trajectory Anti-Aliasing on Guaranteed-Passive Simulation of Nonlinear Physical Systems

Rémy Muller, Thomas Hélie

# TRAJECTORY ANTI-ALIASING ON GUARANTEED-PASSIVE SIMULATION OF NONLINEAR PHYSICAL SYSTEMS

*Rémy Muller, Thomas Hélie* [*]

S3AM team, IRCAM - CNRS UMR 9912- UPMC
1 place Igor Stravinsky, 75004 Paris, France
`remy.muller@ircam.fr`

## ABSTRACT

This article is concerned with the accurate simulation of passive nonlinear dynamical systems with a particular attention paid on aliasing reduction in the pass-band. The approach is based on the combination of Port-Hamiltonian Systems, continuous-time state-space trajectories reconstruction and exact continuous-time anti-aliasing filter realization. The proposed framework is applied on a nonlinear LC oscillator circuit to study the effectiveness of the method.

## 1. INTRODUCTION

The need for accurate and passive-guaranteed simulation of non-linear multi-physical systems is ubiquitous in the modelling of electronic circuits or mechanical systems.

Geometric numerical integration [1] is a very active research field that provides a theoretical framework for structure and invariant preserving integration of dynamical systems. Port-Hamiltonian Systems (PHS) [2] [3] that focus on the energy storage functions and power continuous component interconnections belong to this field and offer a well adapted framework to preserve the system energy (resp. passivity). In the context of nonlinear physical audio systems, it has been applied successfully to the modelling of the wah-wah pedal [4], Fender Rhodes [5], brass instruments [6] and the loudspeaker nonlinearities [7]. Automatic generation of the system equations from a graph of components has been investigated in [8]

However the presence of aliasing errors in the numerical simulation is annoying for three reasons. First it causes audible inharmonic audio artefacts. Second it deteriorates the accuracy of the numerical scheme leading to poor convergence rate. Third it requires the use of significant oversampling. This problem is even more pronounced in the case of systems such as sustained instruments that rely on nonlinearities to achieve auto-oscillation.

Aliasing errors in the context of finite elements simulation and some alternatives have been discussed in [9] (ch 11). Anti-aliased waveform generation without oversampling has been proposed in [10]. Static nonlinearity anti-aliasing has also been proposed in [11] [12] by combining exact anti-derivatives and finite-differences.

Continuous-time input reconstruction has been used in [13] to simulate the frequency response of LTI systems with higher accuracy. It is also central in collocation-based Runge-Kutta methods

that rely on non-uniform polynomial interpolation of the vector field. Splines and in particular uniform B-splines [14] [15] [16], [17] also offer a particularly interesting framework to represent and manipulate piecewise continuous-time signals through their digital representations using the standard tools of linear algebra and digital signal processing.

In this article, we try to combine the geometric and the signal processing viewpoints: we choose a physically informed piecewise smooth polynomial reconstruction model based on a discrete sequence of points generated by a passive-guaranteed simulation method.

The paper is organized as follows. We first recall some results about Port-Hamiltonian systems in Section 3, then we consider passive numerical methods in section 4, we talk about piecewise-continuous trajectory reconstruction in section 5 and continuous-time filtering of piecewise polynomials in section 6. Finally we apply our method to a non linear LC oscillator circuit in section 7.

## 2. PROBLEM STATEMENT

### 2.1. Objective

The objective is to simulate nonlinear passive physical audio systems in such a way that:

(i) The nonlinear dynamics is accurately reproduced,

(ii) The power balance decomposed into its conservative, dissipative and source parts is satisfied,

(iii) The observation operator is designed to reduce the aliasing induced by the nonlinearities.

### 2.2. Approach

To address this problem, the following strategy is adopted.

First, trajectories are approximated in the continuous-time domain by smooth parametric piecewise-defined functions, such that the three following properties are fulfilled:

(P1) Regularity: functions and junctions are $\mathcal{C}^k$ with $k \in \mathbb{N}$,

(P2) Accuracy: the approximation has accuracy order $p$,

(P3) Passivity: the power balance is globally satisfied for each frame.

Second, the anti-aliased output is built *a posteriori* in three steps:

1. Observe the output from the approximated dynamics in the continuous-time domain,

2. Apply a continuous-time anti-aliasing filter in order to respect the Shannon-Nyquist sampling theorem,

3. Sample the filtered trajectories to convert them back to discrete-time.

## 2.3. Methodology

In this article, we restrict ourselves to piece-wise continuous globally $\mathcal{C}^1$ *polynomial* trajectories of the form

$$\hat{\mathbf{x}}(t) = \sum_{n=-\infty}^{\infty} \hat{\mathbf{x}}_n\left(\frac{t-t_n}{h}\right) \operatorname{rect}_{]0,1]}\left(\frac{t-t_n}{h}\right), \quad t \in \mathbb{R} \quad (1)$$

with $\hat{\mathbf{x}} \in \mathbb{R}^N$, $\hat{\mathbf{x}}_n(\tau)$, $\tau \in [0,1]$ being a local polynomial model of order $r$, $t_n = hn$, $n \in \mathbb{Z}$ and $h$ being the time step parameter. The continuity hypothesis (P1) is expressed mathematically by.

$$\hat{\mathbf{x}}_{n+1}^{(\ell)}(\tau) = \hat{\mathbf{x}}_n^{(\ell)}(\tau) \quad \forall n \in \mathbb{Z}, \ell \leq k \quad (2)$$

For property (P2) the local approximation error between the exact solution and its approximation is defined by

$$e(h) = \mathbf{x}(t_0 + h) - \hat{\mathbf{x}}(t_0 + h) \quad (3)$$

provided that $\mathbf{x}(t_0) = \hat{\mathbf{x}}(t_0)$ and it is required that for some $p$.

$$e(h) = \mathcal{O}(h^{p+1}) \quad (4)$$

Finally to express property (P3) we require the power-balance

$$E'(t) = -\mathcal{P}_d + \mathcal{P}_e \quad (5)$$

where $\mathcal{P}_d$ and $\mathcal{P}_e$ are respectively the dissipated and external power and $E'(t)$ is the instantaneous energy variation of the system.

## 3. PORT-HAMILTONIAN SYSTEMS

In this article, nonlinear passive physical audio systems are described under their Port-Hamiltonian formulation. The theory of Port-Hamiltonian Systems (PHS) [2] [3] extends the theory of Hamiltonian mechanics to non-autonomous and dissipative open systems. It provides a general framework where the dynamic state-space equations derives directly from an energy storage function and *power-conserving* interconnection of its subsystems.

### 3.1. Explicit differential form

Consider a system with input $\mathbf{u}(t) \in \mathbb{U} = \mathbb{R}^P$, with state $\mathbf{x}(t) \in \mathbb{X} = \mathbb{R}^N$ and output $\mathbf{y}(t) \in \mathbb{Y} = \mathbb{R}^P$ with the structured state-space equations [2]

$$\begin{cases} \mathbf{x}' &= (\mathbf{J}(\mathbf{x}) - \mathbf{R}(\mathbf{x}))\nabla\mathcal{H}(\mathbf{x}) + \mathbf{G}(\mathbf{x})\mathbf{u} = f(\mathbf{x}, \mathbf{u}) \\ \mathbf{y} &= \mathbf{G}(\mathbf{x})^T\mathbf{u} \end{cases} \quad (6)$$

where $\mathcal{H}$ gives the stored energy of the system

$$E(t) = (\mathcal{H} \circ \mathbf{x})(t) \quad (7)$$

with $\mathcal{H} \in \mathcal{C}^1(\mathbb{X}, \mathbb{R}^+)$, $\nabla$ being the gradient operator, $\mathbf{J} = -\mathbf{J}^T$ a skew-symmetric matrix and $\mathbf{R} = \mathbf{R}^T \succeq 0$ a positive-semidefinite matrix. The energy variation of this system satisfies the power-balance given by the derivative chain rule

$$E'(t) = \nabla\mathcal{H}(\mathbf{x})^T\mathbf{x}' \quad (8)$$

which can be decomposed as

$$E'(t) = \mathcal{P}_c - \mathcal{P}_d + \mathcal{P}_e \quad (9)$$

with.

$$\mathcal{P}_c = \nabla\mathcal{H}(\mathbf{x})^T\mathbf{J}(\mathbf{x})\nabla\mathcal{H}(\mathbf{x}) = 0 \quad (10)$$
$$\mathcal{P}_d = \nabla\mathcal{H}(\mathbf{x})^T\mathbf{R}(\mathbf{x})\nabla\mathcal{H}(\mathbf{x}) \geq 0 \quad (11)$$
$$\mathcal{P}_e = \nabla\mathcal{H}(\mathbf{x})^T\mathbf{G}(\mathbf{x})\mathbf{u} \quad (12)$$

The $\mathcal{P}_c$ term is null because $\mathbf{J}$ is skew-symmetric: it represents conservative power exchange between storage components in the system. The $\mathcal{P}_d$ term is positive because $\mathbf{R} \geq 0$: it represents the dissipated power. Finally the term $\mathcal{P}_e$ represents the power brought to the system by the external ports.

Equation (9) express the system's *passivity property*: with external inputs switched off ($\mathbf{u} = 0$) the energy can either be constant (conservative case $\mathcal{P}_d = 0$) or decaying (dissipative case $\mathcal{P}_d > 0$).

### 3.2. Component-based approach and semi-explicit DAE form

More generally, PHS can be expressed in Differential Algebraic Equation form. When we consider physical systems containing $N$ energy-storage components, $M$ dissipative components and $P$ external interaction ports described by

$\mathcal{P}_c$  the stored energy level $e_n$ and its variation law defined by $e'_n = \nabla\mathcal{H}_n(x_n)x'_n$ for the state variable $x_n$.

$\mathcal{P}_d$  the dissipated power $q_m(w) \geq 0$ with the component's flux and effort variables being in algebraic relation of a single variable $w$.

$\mathcal{P}_e$  the external power $u_p y_p$ brought to the system through this port with $u_p$ being the controllable input of the system and $y_p$ being the observable output.

For a storage component, $e_n = \mathcal{H}_n(x_n)$ gives the physical *energy storage law*. If $x'_n$ is a flux (resp. effort) variable then $\nabla\mathcal{H}_n(x_n)$ is the dual effort (resp. flux) variable.

Similarly, for a dissipative component, the power is $q_m = R_m(w_m)$ so that if $w_m$ is a flux (resp. effort) variable then $z(w_m) = \frac{R_m(w_m)}{w_m}$ is the effort (resp. flux) and gives the *dissipation law*.

We then consider a passive system obtained by interconnection of these components given by

$$\underbrace{\begin{bmatrix} \mathbf{x}' \\ \mathbf{w} \\ -\mathbf{y} \end{bmatrix}}_{\mathbf{b}} = \mathbf{S}(\mathbf{x}, \mathbf{w}) \underbrace{\begin{bmatrix} \nabla\mathcal{H}(\mathbf{x}) \\ z(\mathbf{w}) \\ \mathbf{u} \end{bmatrix}}_{\mathbf{a}} \quad (13)$$

with $\mathbf{S} = -\mathbf{S}^T$ being skew-symmetric, $\mathcal{H}(\mathbf{x}) = \sum_{i=1}^N \mathcal{H}_n(x_n)$ and $z(\mathbf{w}) = [z_1(w_1), \ldots, z_m(w_m)]^T$.

The $\mathbf{S}$ matrix represents the power exchange between components: since $\mathbf{S} = -\mathbf{S}^T$ we have $\mathbf{a} \cdot \mathbf{b} = \mathbf{a}^T\mathbf{Sa} = 0$ which again leads to the power balance[1].

$$\underbrace{\nabla\mathcal{H}(\mathbf{x}) \cdot \mathbf{x}'}_{\mathcal{P}_c = E'(t)} + \underbrace{z(\mathbf{w}) \cdot \mathbf{w}}_{\mathcal{P}_d} - \underbrace{\mathbf{u} \cdot \mathbf{y}}_{\mathcal{P}_e} = 0 \quad (14)$$

The explicit form (6) can be found by solving the second row of (13). The $\mathbf{S}$ matrix represents a *Dirac structure* [2] that expresses the power-balance and can be constructed from a component connection graph [8] [18].

---

[1]The minus sign in $-y$ in Eq. (13) is used to restore the receiver convention used for internal components.

## 4. PASSIVE NUMERICAL INTEGRATION

Whereas most numerical schemes concentrate their efforts on the the temporal derivative or the numerical integration quadrature, discrete gradient methods preserve the energy (resp. passivity) given by the power-balance (9), (14) in discrete-time by providing a discrete equivalent of the chain rule derivation property $E'(t) = \nabla\mathcal{H}(\mathbf{x})^T\mathbf{x}'$. A discrete gradient [19] $\overline{\nabla}H$ is required to satisfy the following conditions.

$$\mathcal{H}(\mathbf{x} + \delta\mathbf{x}) - \mathcal{H}(\mathbf{x}) = \overline{\nabla}\mathcal{H}(\mathbf{x}, \delta\mathbf{x})^T\delta\mathbf{x} \qquad (15)$$

$$\overline{\nabla}\mathcal{H}(\mathbf{x}, 0) = \nabla\mathcal{H}(\mathbf{x}) \qquad (16)$$

In this article, we will focus on the average vector field [20].

### 4.1. Average Vector Field

In the general case, the AVF method is defined by.

$$\frac{\delta\mathbf{x}_n}{\delta t} = \int_0^1 f(\mathbf{x}_n + \tau\delta\mathbf{x}_n)d\tau, \quad \mathbf{x}_{n+1} = \mathbf{x}_n + \delta\mathbf{x}_n \qquad (17)$$

When the matrices $\mathbf{J}(\mathbf{x}), \mathbf{R}(\mathbf{x}), \mathbf{G}(\mathbf{x})$ are approximated by constant matrices $\bar{\mathbf{J}}, \bar{\mathbf{R}}, \bar{\mathbf{G}}$, we obtain the separable structure-preserving approximation of (17)

$$\frac{\delta\mathbf{x}_n}{\delta t} = (\bar{\mathbf{J}} - \bar{\mathbf{R}})\overline{\nabla}H(\mathbf{x}_n, \delta\mathbf{x}_n) + \bar{\mathbf{G}}\bar{\mathbf{u}}_n \qquad (18)$$

with the discrete gradient being defined by

$$\overline{\nabla}\mathcal{H}(\mathbf{x}, \delta\mathbf{x}) = \int_0^1 \nabla\mathcal{H}(\mathbf{x} + \tau\delta\mathbf{x})d\tau \qquad (19)$$

and it satisfies the *discrete power balance*

$$\delta E = \overline{\nabla}\mathcal{H}^T\frac{\delta\mathbf{x}}{\delta t} = \overline{\nabla}\mathcal{H}^T(\bar{\mathbf{J}} - \bar{\mathbf{R}})\overline{\nabla}\mathcal{H} + \overline{\nabla}\mathcal{H}^T\bar{\mathbf{G}}\bar{\mathbf{u}}$$
$$= 0 - \mathcal{P}_d + \mathcal{P}_e$$

Then, by the fundamental theorem of calculus, for mono-variant components, i.e. separable Hamiltonians of the form $\mathcal{H}(\mathbf{x}) = \sum_{i=1}^N \mathcal{H}_i(x_i)$, we have for each coordinate:

$$\overline{\nabla}\mathcal{H}_i(x_i, \delta x_i) = \begin{cases} \frac{\mathcal{H}_i(x_i + \delta x_i) - \mathcal{H}_i(x_i)}{\delta x_i} & \delta x_i \neq 0 \\ \nabla\mathcal{H}(x_i) & \delta x_i = 0 \end{cases} \qquad (20)$$

which satisfies the discrete gradient conditions (15)-(16). For non-separable Hamiltonians, a discrete-gradient can also be uniquely defined, see [21] for more details.

To summarize, this method relies on two complimentary approximations: the differential operator $\frac{d\mathbf{x}}{dt} \to \frac{\delta\mathbf{x}}{\delta t}$ and the vector field $f \to \overline{f}$ to achieve energy (resp. passivity) conservation. The discrete PHS equivalent of (6) is given by the numerical scheme.

$$\begin{cases} \frac{\delta\mathbf{x}_n}{\delta t} & = (\bar{\mathbf{J}} - \bar{\mathbf{R}})\,\overline{\nabla}\mathcal{H}(\mathbf{x}_n, \delta\mathbf{x}_n) + \bar{\mathbf{G}}\bar{\mathbf{u}}_n \\ \mathbf{y}_n & = \bar{\mathbf{G}}^T\overline{\nabla}\mathcal{H}(\mathbf{x}_n, \delta\mathbf{x}_n) \\ \mathbf{x}_{n+1} & = \mathbf{x}_n + \delta\mathbf{x}_n \end{cases} \qquad (21)$$

### 4.2. Accuracy order

As shown in [22], the AVF has accuracy order $p = 2$, it is a B-series method, is affine-covariant and self-adjoint. When approximated as in Eq (19) by evaluating matrices $\mathbf{J}, \mathbf{R}, \mathbf{G}$ for $\mathbf{x}^* = \mathbf{x}_n$ the accuracy is only of order 1. Order 2 is achieved when either $\mathbf{J}, \mathbf{R}, \mathbf{G}$ are independent of $\mathbf{x}$ or when evaluated at the mid-point $\mathbf{x}^* = \mathbf{x}_n + \frac{\delta\mathbf{x}_n}{2}$ in the conservative case. It is also possible to restore the accuracy order $p = 2$ in the general case using a Runge-Kutta refinement [21].

### 4.3. Implicit resolution

The discrete system is implicit on $\delta\mathbf{x}_n$ and admits a unique solution when $\mathcal{H}$ is convex. In the general case, an iterative solver is required (typically a fixed-point or Newton iteration), but when the Hamiltonian is quadratic we can avoid the need for an iterative resolution. Furthermore, when the Hamiltonian is convex the method can also be made non-iterative by quadratization of the Hamiltonian [21].

*Proof.* When the Hamiltonian is quadratic of the form $\mathcal{H}(\mathbf{x}) = \frac{1}{2}\mathbf{x}^T\mathbf{Q}\mathbf{x}$, the discrete gradient reduces to the mid-point rule

$$\overline{\nabla}\mathcal{H}(\mathbf{x}, \delta\mathbf{x}) = \int_0^1 \mathbf{Q}(\mathbf{x}_n + \delta\mathbf{x}_n\tau)d\tau = \mathbf{Q}\left(\mathbf{x}_n + \frac{1}{2}\delta\mathbf{x}_n\right)$$

the implicit dependency on $\delta\mathbf{x}$ can thus be solved by matrix inversion

$$\delta\mathbf{x}_n = \delta t\left(I - \frac{\delta t}{2}\mathbf{A}\right)^{-1}\left(\mathbf{A}\mathbf{x}_n + \bar{\mathbf{G}}\bar{\mathbf{u}}_n\right) \qquad (22)$$

with $\mathbf{A} = (\bar{\mathbf{J}} - \bar{\mathbf{R}})\mathbf{Q}$ $\qquad\qquad\qquad\qquad\qquad\square$
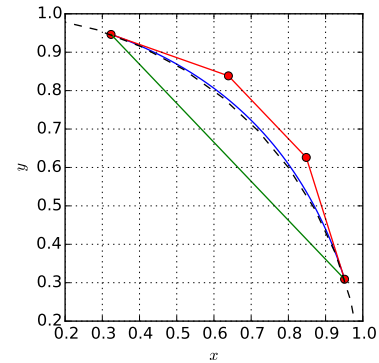
## 5. PIECEWISE-CONTINUOUS TRAJECTORIES



*Figure 1: Example of a cubic trajectory with conservative endpoints. The affine trajectory used to compute the average vector field is shown (in green), the associated cubic interpolated approximation (in blue), its control polygon (in red), and the exact manifold (in dashed black).*

Given the sequence of points $\{\mathbf{x}_n\}$ obtained by a passive-guaranteed method, we would like to reconstruct piece-wise $\mathcal{C}^k$-continuous polynomial trajectories informed by the system dynamics.

The idea is to exploit the dynamic equation at each junction point $\mathbf{x}_n$ where the approximation is known to be $\mathcal{O}(h^{p+1})$.

Indeed, if we had the samples of the exact trajectory, by the Weierstrass approximation theorem, arbitrarily close polynomial approximations converging uniformly to the exact solution could be obtained by computing its derivatives to any desired order.

Since we only have an approximation of order $p = 2$, we restrict ourselves to a regularity $k = 1$. This gives four constraints

$$\hat{\mathbf{x}}(0) = \mathbf{x}_n, \quad \hat{\mathbf{x}}(1) = \mathbf{x}_{n+1}, \quad \hat{\mathbf{x}}'(0) = f(\mathbf{x}_n), \quad \hat{\mathbf{x}}'(1) = f(\mathbf{x}_{n+1})$$

that can be satisfied by a cubic polynomial ($r = 3$). We choose to represent it using the Bézier form,

$$\hat{\mathbf{x}}(\tau) = \sum_{i=0}^{3} \mathbf{X}_i B_i^3(\tau), \quad B_i^n(t) = \binom{n}{i}(1-t)^{n-i}t^i \quad (23)$$

with $\{\mathbf{X}_i\}$ being its control polygon and $B_i^n(t)$ being the Bernstein polynomial basis functions, because they have important geometric and finite differences interpretations [23].

This choice immediately leads to the following equations,

$$\mathbf{X}_0 = \mathbf{x}_n \qquad \mathbf{X}_1 = \mathbf{x}_n + \frac{1}{3}f(\mathbf{x}_n) \qquad (24)$$

$$\mathbf{X}_3 = \mathbf{x}_{n+1} \qquad \mathbf{X}_2 = \mathbf{x}_{n+1} - \frac{1}{3}f(\mathbf{x}_{n+1}) \qquad (25)$$

where the internal control points $\mathbf{X}_1, \mathbf{X}_2$ are computed from the end points $\mathbf{x}_n, \mathbf{x}_{n+1}$ by first order forward / backward prediction using the derivative rule.

$$\hat{\mathbf{x}}'(t) = \sum_{i=0}^{n-1} \mathbf{D}_i B_i^{n-1}(t), \quad \mathbf{D}_i = n(\mathbf{X}_{i+1} - \mathbf{X}_i) \qquad (26)$$

An example trajectory is shown in Figure 1.

## 6. ANTI-ALIASED OBSERVATION

Given an observed signal $\tilde{\mathbf{u}}(t) = \mathbf{y}(t)$ belonging to the class of piecewise polynomials, in order to reject the non-band-limited part of the spectrum, we would like to apply an antialiasing filter operator given by its continuous-time ARMA transfer function $H(s)$, then sample its output $\tilde{y}(t)$ to get back to the digital domain.

Since our anti-aliasing filter will be LTI, we will make use of *exact exponential integration* and decompose its output on a *custom basis* of exponential polynomial functions.

Without loss of generality we only consider single-input single-output filters (SISO) since we can always filter each observed output independently.

### 6.1. State-space ARMA filtering of polynomial input

We want to filter the trajectory by an ARMA filter given by its Laplace transfer function

$$H(s) = \frac{Y(s)}{U(s)} = \frac{b_0 s^N + b_1 s^{N-1} + \ldots + b_N}{s^N + a_1 s^{N-1} + \ldots + a_N} \qquad (27)$$

This filter can be realized in state-space form as

$$\tilde{\mathbf{x}}' = \mathbf{A}\tilde{\mathbf{x}} + \mathbf{B}\tilde{u} \qquad (28)$$

$$\tilde{y} = \mathbf{C}\tilde{\mathbf{x}} + \mathbf{D}\tilde{u} \qquad (29)$$

Common choices are the observable and controllable state-space forms.

Furthermore when the denominator can be factored with distinct roots, it is possible to rewrite the transfer function using partial fraction expansion as.

$$H(s) = c_0 + \frac{c_1}{s - \lambda_1} + \ldots + \frac{c_N}{s - \lambda_N} \qquad (30)$$

which leads to the canonical diagonal form

$$\mathbf{A} = \begin{bmatrix} \lambda_1 & & \\ & \ddots & \\ & & \lambda_N \end{bmatrix} \qquad \mathbf{B} = \begin{bmatrix} 1 \\ \vdots \\ 1 \end{bmatrix} \qquad (31)$$

$$\mathbf{C} = \begin{bmatrix} c_1 & \ldots & c_N \end{bmatrix} \qquad \mathbf{D} = \begin{bmatrix} c_0 \end{bmatrix} \qquad (32)$$

### 6.2. Exact exponential integration

The exact state trajectory is given by the integral

$$\tilde{\mathbf{x}}(t) = \tilde{\mathbf{x}}_h(t) + \tilde{\mathbf{x}}_e(t) = e^{\mathbf{A}t}\tilde{\mathbf{x}}_0 + \int_0^t e^{\mathbf{A}(t-\tau)}\mathbf{B}\tilde{u}(\tau)d\tau \quad (33)$$

as the sum of the homogeneous solution to the initial conditions $\tilde{\mathbf{x}}_h$ and the forced state-response with zero initial conditions $\tilde{\mathbf{x}}_e$ given by the convolution of the input with the kernel $e^{\mathbf{A}t}$.

Furthermore when $\mathbf{A}$ is diagonal we have

$$e^{\mathbf{A}t} = \begin{bmatrix} e^{\lambda_1 t} & & \\ & \ddots & \\ & & e^{\lambda_N t} \end{bmatrix} \qquad (34)$$

which greatly simplifies the computation of the exponential map. In that case (33) can be evaluated component-wise as

$$\tilde{x}^i(t) = e^{\lambda_i t}\tilde{x}_0^i + \int_0^t e^{\lambda_i(t-\tau)}\tilde{u}(\tau)d\tau \quad i \in \{1 \ldots N\} \quad (35)$$

where we used the notation $x^i$ to detonate the $i$-th coordinate of the vector $\mathbf{x}$

#### 6.2.1. Polynomial input

With $\tilde{u}(t)$ being a polynomial of degree $K$ in monomial[2] form and coefficients $\tilde{u}_k$

$$\tilde{u}(t) = \sum_{k=0}^{K} \tilde{u}_k \frac{t^k}{k!} \qquad (36)$$

we can expand the forced response $\tilde{x}_e$ in (35) as a weighted sum

$$\int_0^t e^{\lambda_i(t-\tau)} \left( \sum_{k=0}^{K} \tilde{u}_k \frac{t^k(\tau)}{k!} \right) d\tau = \sum_{k=0}^{K} \tilde{u}_k \varphi_{k+1}(\lambda_i, t) \quad (37)$$

with the basis functions $\{\varphi_k\}$ being defined by the convolution

$$\varphi_k(\lambda, t) = \int_0^t e^{\lambda(t-\tau)} \frac{\tau^{k-1}}{(k-1)!} d\tau \qquad k \geq 1 \qquad (38)$$

One of the main advantages of using a polynomial input (rather than a more general model) lies in the fact that these basis functions can be integrated exactly, avoiding the need of a quadrature
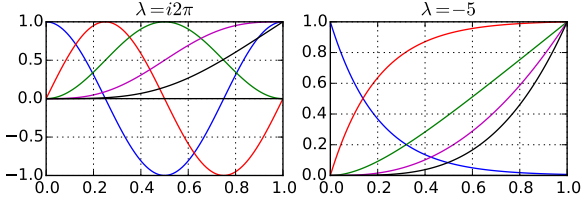
*Figure 2: Normalized $\varphi$-functions for $k \in \{0 \ldots 4\}$. The real parts of the impulse (blue), step (red), ramp (green), quadratic (magenta) and cubic (black) responses are shown for a complex pole $\lambda = i2\pi$ (left plot) and a real pole $\lambda = -5$ (right plot) over the unit interval $t \in [0, 1]$.*

approximation formula. See Appendix 12 for a detailed derivation and a recursive formula, and Figure 2 for their temporal shapes.

Using those we can decompose the local state trajectories as.

$$\tilde{x}^i(t) = \tilde{x}_0^i \varphi_0(\lambda_i, t) + \sum_{k=0}^{K} \tilde{u}_k \varphi_{k+1}(\lambda_i, t) \qquad (39)$$

We note that the initial condition is equivalent to an impulsive input $\tilde{x}_0^i \delta(t)$. This filtering scheme can thus be generalized to non polynomial impulsive inputs.

#### 6.2.2. Numerical update scheme

Since we only wish to sample the trajectory on a fixed grid $t_n \in \mathbb{Z}$, we just need to evaluate the local state trajectory $\mathbf{x}(t)$ and the output $y(t)$ at $t = 1$ to finally get the following numerical scheme

$$\tilde{x}_{n+1}^i = \tilde{x}_n^i \varphi_0(\lambda_i) + \sum_{k=0}^{K} \tilde{u}_{k,n} \varphi_{k+1}(\lambda_i, 1) \qquad (40)$$

$$\tilde{y}_{n+1} = \sum_{i=1}^{N} c_i \tilde{x}_{n+1}^i + c_0 \tilde{u}_n(1) \qquad (41)$$

where the coefficients $\varphi_k(\lambda_i, 1)$ can be pre-computed and the components $\tilde{x}_{n+1}^i$ evaluated in parallel.

### 6.3. Filter examples

#### 6.3.1. Low-pass filter of order 1

We consider a first order low-pass filter with transfer function $H(s) = \frac{a}{s+a}$. The temporal response to a piecewise polynomial input $\{t^2, 1 - t, 0, 1\}$ is shown in Figure 3 for $a \in \{1, 3, 6, 10\}$.

#### 6.3.2. Butterworth Filter of order 3

To further illustrate the non-band-limited representation capacity of piece-wise polynomials, and the effectiveness of the filtering scheme, we have shown in Figure 4 the response of a third-order Butterworth filter with cutoff $\omega_c = \pi$ to a triangular input signal. Its Laplace transfer function for a normalized pulsation $\omega_c = 1$ is given by $H(s) = \frac{1}{(s^2+s+1)(s+1)}$ with poles $\lambda_1 = \frac{-1-i\sqrt{3}}{2}$, $\lambda_2 = \frac{-1+i\sqrt{3}}{2}$, $\lambda_3 = -1$ and coefficients $c_0 = 0$, $c_1 = \frac{-3+i\sqrt{3}}{6}$, $c_2 = \frac{-3-i\sqrt{3}}{6}$, $c_3 = 1$.

---

[2] We use the monomial form here instead of Bernstein polynomials because this is the one that leads to the most straightforward and meaningful derivation.
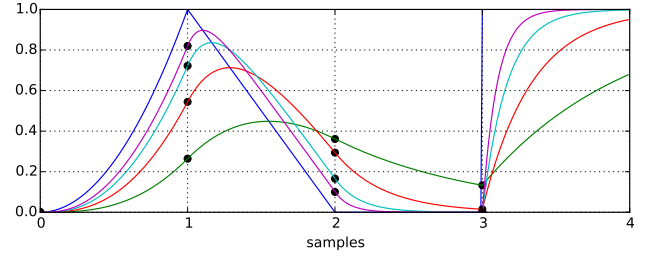


*Figure 3: Exact continuous-time responses of a first order low-pass filter to a polynomial input (in blue).*
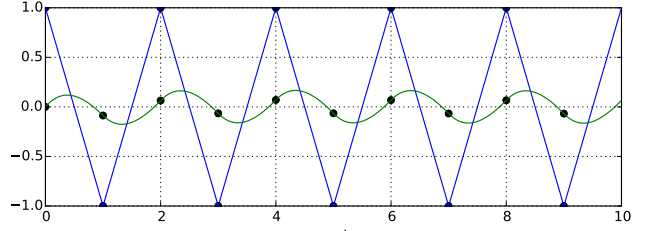


*Figure 4: Exact continuous-time response of the order 3 Butterworth filter with cutoff pulsation $\omega_c = \pi$ to a triangle input at the Nyquist frequency.*

## 7. APPLICATION: NONLINEAR LC OSCILLATOR

In order to illustrate the proposed method, we consider the simplest example having non linear dynamics. For that purpose, we use a parallel autonomous LC circuit with a linear inductor and a saturating capacitor with the Hamiltonian energy storage function given by

$$\mathcal{H}(q, \phi) = \frac{\ln(\cosh(q))}{C_0} + \frac{\phi}{2L} \qquad (42)$$

where the state $q$ is the charge of the capacitor and $\phi$ the flux in the inductor. Its circuit's schematic is shown in figure 5 and its energy storage law are displayed in 6
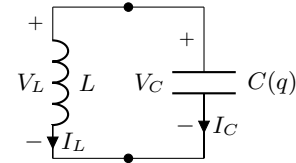


*Figure 5: A nonlinear LC oscillator circuit*

By partial differentiation of the Hamiltonian function $\mathcal{H}$ by respectively $q$ and $\phi$ we get the capacitor's voltage and the inductor's current, while applying the temporal derivative on $q$, $\phi$ gives the capacitor's current and inductor's voltage.

$$V_C = \partial_q \mathcal{H} = \frac{\tanh(q)}{C_0} \qquad\qquad I_C = q' \qquad (43)$$

$$I_L = \partial_\phi \mathcal{H} = \frac{\phi}{L} \qquad\qquad V_L = \phi' \qquad (44)$$
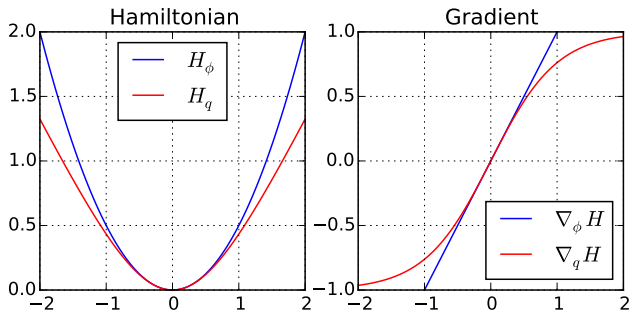
*Figure 6: Respective energy storage functions (left plot) and their gradients (right plot), of the nonlinear capacitor (in red) and linear inductor (in blue), for $C = 1$, $L = 1$.*
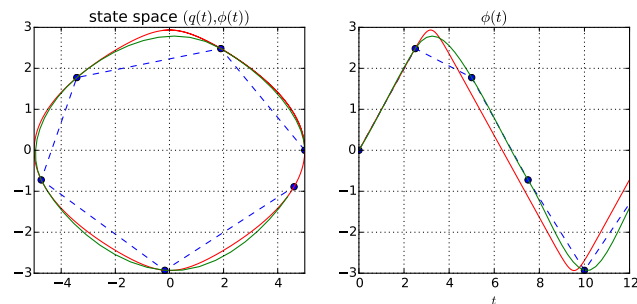


*Figure 7: Comparison of simulated orbits with discrete points (in blue) computed using the AVF method, reconstructed cubic trajectory (in green) and reference trajectory computed at 10x sampling rate (in red).*



*Figure 8: Continuous-time spectrum of the nonlinear LC circuit flux $\phi$ for a fundamental frequency of 500 Hz and a sampling frequency of 44.1 kHz. The 10x oversampled reference is compared to the AVF method's discrete output with zero-order hold (ZOH), first-order hold (FOH), the proposed method (proposed cubic) and its 12th order Butterworth filtered spectrum (proposed + AA). The Nyquist frequency is materialized in blue and the multiples of the sampling rate in red.*

This gives the Branch Component Equations.

Applying Kirchhoff Current and Voltage Laws gives the constraints $I_C = -I_L$, $V_C = V_L$. We can summarize the previous equations with the conservative autonomous Hamiltonian system.

$$\mathbf{x}' = \mathbf{J} \nabla \mathcal{H}(\mathbf{x}) \qquad (45)$$

with.

$$\mathbf{x} = \begin{bmatrix} q \\ \phi \end{bmatrix}, \qquad \mathbf{J} = \begin{bmatrix} 0 & -1 \\ 1 & 0 \end{bmatrix}, \qquad \nabla \mathcal{H} = \begin{bmatrix} \partial_q \mathcal{H} \\ \partial_\phi \mathcal{H} \end{bmatrix} \qquad (46)$$

Its state space and temporal trajectories are shown in Figure 7. We can see that the numerical scheme preserves the energy since the discrete points lie exactly on the orbit of the reference trajectory. The reconstructed state-space trajectory also shows a good match with the reference for most of the interpolated segments, except around transition regions at the bottom and top.

The spectrum of the flux $\phi$ is shown in Figure 8. One can see that the reference spectrum contains harmonics above twice the representable bandwidth where they pass below -90 dB.

The ZOH and FOH spectrums contains spectral images of the non bandlimited spectrum that decay respectively at -6dB/oct and -12dB/oct. Their aliased components in the audio bandwidth start around -80 dB at the Nyquist frequency and decay slowly toward approximately -100 dB at low frequencies.

Contrary, our method, informed by the dynamic, exhibits both reduced aliasing in the audio bandwidth and sharpened spectrum
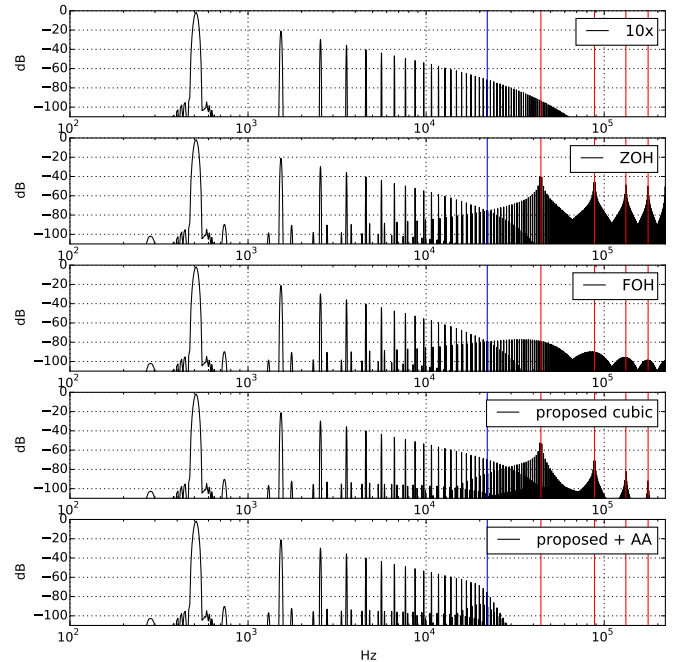
around the Nyquist frequency. It also has a higher spectral images decay rate thanks to its $\mathcal{C}^1$ regularity. Its aliased components start at -85 dB at the Nyquist frequency and decay much faster to reach -100 dB at about 14 kHz where they reach a kind of aliasing noise floor caused by higher harmonics fold-back.

Finally, as expected, the 12th-order Butterworth half-band lowpass filter removes components above the Nyquist frequency thanks to the piecewise continuous cubic input.

## 8. DISCUSSION

First, we highlight the fact that the vector field approximation in (17) acts as a first-order antialiasing filter: it is a projection of the vector field on a rectangular kernel. It prevents high-order spectral images from disturbing the low frequency dynamic during the numerical simulation and it is consistent with the underlying piecewise linear approximation model.

Second, the numerical scheme is energy-preserving. From a signal processing perspective, the lowpass filtering effect on the vector field is compensated by the finite difference approximation of the derivative. This is a direct generalization of the mid-point / bilinear methods to nonlinear differential equations.

Third, using the fact that the trajectory approximation has accuracy order $p = 2$ at the junctions, we can re-exploit the differential equation to reconstruct an informed $\mathcal{C}^1$-continuous cubic trajectory. It exhibits reduced aliasing in the passband and better

high-frequency resolution.

We observe that on the studied example, our method manages to reduce aliased components that are folded once into the audio band. However components caused by multiple folding of the spectrum cannot be removed anymore. This is related to the Papoulis generalized sampling expansion [24] who states that a band-limited function can be perfectly reconstructed from its values and derivatives sampled at half the Nyquist rate.

Some difficulties arise when trying to generalize the above ideas to higher order trajectories and filtering kernels. First, the line-integral (17) is no longer computable in closed form when the trajectory model is non-affine. Second, higher order kernels have longer temporal support which can lead to non-causal integrals.

## 9. CONCLUSION AND PERSPECTIVES

Our main contribution is an approach based on smooth piecewise defined trajectories coupled with a guaranteed-passive simulation. The method proceeds in three steps: 1) an energy-preserving passive numerical scheme is applied, 2) $C^k$-continuous trajectories are reconstructed, 3) Exact continuous time lowpass filtering and sampling is performed. We have proposed a first instance of this method using the class of piecewise polynomials with regularity $k = 1$ and accuracy order $p = 2$ that exhibits reduced aliasing.

Further work will concern increasing the regularity $k$ and accuracy order $p$, merging the numerical scheme and the interpolation steps by considering energy-preserving methods with a built-in regular continuous model and considering other classes of models such as rational and exponential functions.

In this regard, exponential integrators [25] that integrate the linear part of the dynamic exactly (as we have done in section 6) and rely on approximations for the nonlinear part are of great interest.

Finally we would like to further investigate the link between multi-stages / multi-derivatives general linear methods, their accuracy orders, numerical dispersion and internal bandwidth, and to analyze their behavior and representation capabilities within the framework of Reproducing Kernels Hilbert Spaces and generalized sampling theory [26] [27] [28].

## 10. ACKNOWLEDGMENTS

## 11. REFERENCES

[1] E. Hairer, C. Lubich, and G. Wanner, *Geometric Numerical Integration: Structure-Preserving Algorithms for Ordinary Differential Equations; 2nd ed.*, Springer, Dordrecht, 2006.

[2] A. van der Schaft and D. Jeltsema, "Port-hamiltonian systems theory: An introductory overview," *Foundations and Trends in Systems and Control*, vol. 1, no. 2-3, pp. 173–378, 2014.

[3] A. van der Schaft, "Port-hamiltonian systems: an introductory survey," in *Proceedings of the International Congress of Mathematicians Vol. III: Invited Lectures*, Madrid, Spain, 2006, pp. 1339–1365.

[4] A. Falaize and T. Hélie, "Simulation of an analog circuit of a wah pedal: a port-Hamiltonian approach," in *135th convention of the Audio Engineering Society*, New-York, United States, Oct. 2013, pp. –.

[5] A. Falaize and T. Hélie, "Passive simulation of the nonlinear port-Hamiltonian modeling of a Rhodes Piano," *Journal of Sound and Vibration*, vol. 390, pp. 289–309, Mar. 2017.

[6] N. Lopes and T. Hélie, "Energy Balanced Model of a Jet Interacting With a Brass Player's Lip," *Acta Acustica united with Acustica*, vol. 102, no. 1, pp. 141–154, 2016.

[7] A. Falaize and T. Hélie, "Passive simulation of electro-dynamic loudspeakers for guitar amplifiers: a port- Hamiltonian approach," in *International Symposium on Musical Acoustics*, Le Mans, France, July 2014, pp. 1–5.

[8] A. Falaize and T. Hélie, "Passive guaranteed simulation of analog audio circuits: A port-hamiltonian approach," *Applied Sciences*, vol. 6, no. 10, 2016.

[9] J. P. Boyd, *Chebyshev and Fourier Spectral Methods*, Dover Books on Mathematics. Dover Publications, Mineola, NY, second edition, 2001.

[10] T. S. Stilson, *Efficiently-variable Non-oversampled Algorithms in Virtual-analog Music Synthesis: A Root-locus Perspective*, Ph.D. thesis, 2006.

[11] V. Zavalishin J. D. Parker and E. Le Bivic, "Reducing the aliasing of nonlinear waveshaping using continuous-time convolution," in *Proc. Digital Audio Effects (DAFx-16)*.

[12] S. Bilbao, F. Esqueda J. D. Parker, and V. Valimaki, "Antiderivative antialiasing for memoryless nonlinearities," in *IEEE Signal Processing Letters*, Nov. 2016.

[13] S. Sarkka and A. Huovilainen, "Accurate discretization of analog audio filters with application to parametric equalizer design," *IEEE Transactions on Audio, Speech, and Language Processing*, vol. 19, no. 8, pp. 2486–2493, Nov 2011.

[14] M. Unser, "Think analog, act digital," in *Seventh Biennial Conference, 2004 International Conference on Signal Processing and Communications (SPCOM'04)*, Bangalore, India, December 11-14, 2004.

[15] M. Unser, A. Aldroubi, and M. Eden, "B-Spline signal processing: Part I—Theory," *IEEE Transactions on Signal Processing*, vol. 41, no. 2, pp. 821–833, February 1993.

[16] M. Unser, A. Aldroubi, and M. Eden, "B-Spline signal processing: Part II—Efficient design and applications," *IEEE Transactions on Signal Processing*, vol. 41, no. 2, pp. 834–848, February 1993.

[17] M. Unser, "Cardinal exponential splines: Part II—Think analog, act digital," *IEEE Transactions on Signal Processing*, vol. 53, no. 4, pp. 1439–1449, April 2005.

[18] A. Falaize, N. Lopes, T. Hélie, D. Matignon, and B. Maschke, "Energy-balanced models for acoustic and audio systems: a port-Hamiltonian approach," in *Unfold Mechanics for Sounds and Music*, Paris, France, Sept. 2014.

[19] E. L. Mansfield and G. R. W. Quispel, "On the construction of discrete gradients," 2009.

[20] E. Celledoni, V. Grimm, R.I. McLachlan, D.I. McLaren, D. O'Neale, B. Owren, and G.R.W. Quispel, "Preserving

energy resp. dissipation in numerical PDEs using the 'average vector field' method," *Journal of Computational Physics*, vol. 231, no. 20, pp. 6770 – 6789, 2012.

[21] N. Lopes, T. Hélie, and A. Falaize, "Explicit second-order accurate method for the passive guaranteed simulation of port-Hamiltonian systems," in *5th IFAC Work- shop on Lagrangian and Hamiltonian Methods for Non Linear Control*, Lyon, France, July 2015, IFAC.

[22] E. Celledoni, R. I. McLachlan, D. I. McLaren, B. Owren, G. R. W. Quispel, and W. M. Wright, "Energy-preserving runge-kutta methods," *ESAIM: Mathematical Modelling and Numerical Analysis*.

[23] R. T. Farouki, "The bernstein polynomial basis: A centennial retrospective," *Comput. Aided Geom. Des.*, vol. 29, no. 6, pp. 379–419, Aug. 2012.

[24] A. Papoulis, "Generalized sampling expansion," *IEEE Transactions on Circuits and Systems*, vol. 24, no. 11, pp. 652–654, Nov 1977.

[25] M. Hochbruck and A. Ostermann, "Exponential integrators," *Acta Numerica*, vol. 19, pp. 209–286, 2010.

[26] D. Nehab and H. Hoppe, "A fresh look at generalized sampling," *Foundations and Trends in Computer Graphics and Vision*, vol. 8, no. 1, pp. 1–84, 2014.

[27] P.L. Dragotti, M. Vetterli, and T. Blu, "Sampling moments and reconstructing signals of finite rate of innovation: Shannon meets strang-fix," *IEEE Transactions on Signal Processing*, vol. 55, no. 5, pp. 1741–1757, May 2007.

[28] M. Unser, "Sampling-50 years after shannon," *Proceedings of the IEEE*, vol. 88, no. 4, pp. 569–587, April 2000.

## 12. APPENDIX: $\varphi$-FUNCTIONS

The $\varphi$-functions, that appear when doing exact integration of an LTI system with polynomial input given in monomial form, are defined by the convolution integral

$$\varphi_k(\lambda, t) = \int_0^t e^{\lambda(t-\tau)} \frac{\tau^{k-1}}{(k-1)!} d\tau \qquad k \geq 1 \qquad (47)$$

and by definition

$$\varphi_0(\lambda, t) := e^{\lambda t} \qquad (48)$$

For $\lambda = 0$ it is immediate that

$$\varphi_k(\lambda = 0, t) = \frac{t^k}{k!} \qquad (49)$$

### 12.1. Recurrence relation

We first prove that they satisfy the recurrence formula

$$\varphi_{k+1}(\lambda, t) = \frac{\varphi_k(\lambda, t) - \varphi_k(0, t)}{\lambda} \qquad \lambda \neq 0 \qquad (50)$$

*Proof.* Using integration by parts

$$\int_a^b u(\tau) v'(\tau) d\tau = [uv]_a^b - \int_a^b u'(\tau) v(\tau) d\tau$$

with $[a, b] = [0, t]$, $u(\tau) = e^{\lambda(t-\tau)}$, $v'(\tau) = \frac{\tau^{k-1}}{(k-1)!}$ and its primitive $v(\tau) = \frac{\tau^k}{k!}$ gives

$$\varphi_k(\lambda, t) = \left[ e^{\lambda(t-\tau)} \frac{\tau^k}{k!} \right]_0^t + \lambda \int_0^t e^{\lambda(t-\tau)} \frac{\tau^k}{k!} d\tau$$

$$= \frac{t^k}{k!} + \lambda \varphi_{k+1}(\lambda, t)$$

which after using (49) and identification gives

$$\varphi_{k+1}(\lambda, t) = \frac{\varphi_k(\lambda, t) - \varphi_k(0, t)}{\lambda}$$

$\square$

### 12.2. Explicit form

Using (50) recursively for $\lambda \neq 0$, the first basis functions are given by

$$\varphi_0(\lambda, t) = e^{\lambda t} \qquad (51)$$

$$\varphi_1(\lambda, t) = \frac{e^{\lambda t} - 1}{\lambda} \qquad (52)$$

$$\varphi_2(\lambda, t) = \frac{e^{\lambda t} - (1 + \lambda t)}{\lambda^2} \qquad (53)$$

$$\varphi_3(\lambda, t) = \frac{e^{\lambda t} - (1 + \lambda t + \frac{(\lambda t)^2}{2!})}{\lambda^3} \qquad (54)$$

$$\varphi_4(\lambda, t) = \frac{e^{\lambda t} - (1 + \lambda t + \frac{(\lambda t)^2}{2!} + \frac{(\lambda t)^3}{3!})}{\lambda^4} \qquad (55)$$

this suggests the following explicit form

$$\varphi_k(\lambda, t) = \frac{1}{\lambda^k} \left( e^{\lambda t} - \sum_{n=0}^{k-1} \frac{(\lambda t)^n}{n!} \right), \quad \lambda \neq 0 \qquad (56)$$

*Proof.* It is immediate to verify that (56) is satisfied for $k = 0$. Then assuming that (56) is true for some $k \in \mathbb{N}$ and using the recurrence (50) we prove

$$\varphi_{k+1}(\lambda, t) = \frac{\varphi_k(\lambda, t) - \varphi_k(0, t)}{\lambda}$$

$$= \frac{1}{\lambda^{k+1}} \left( e^{\lambda t} - \sum_{n=0}^{k-1} \frac{(\lambda t)^n}{n!} \right) - \frac{1}{\lambda} \frac{t^k}{k!}$$

$$= \frac{1}{\lambda^{k+1}} \left( e^{\lambda t} - \sum_{n=0}^{k} \frac{(\lambda t)^n}{n!} \right)$$

that (56) is also true for $k + 1$. By induction (56) is thus satisfied for all $k \in \mathbb{N}$. $\square$

The $\varphi$-functions represent thus the tail of the truncated taylor series expansion of $e^{\lambda t}$ up to a scaling factor. This is clear when rewriting (56) as

$$e^{\lambda t} = \sum_{n=0}^{k-1} \frac{(\lambda t)^n}{n!} + \lambda^k \varphi_k(\lambda, t) \qquad (57)$$